Design and validation of a wireless Body Sensor Network for integrated EEG and HD-sEMG acquisitions

Design and Validation of a Wireless Body Sensor Network for Integrated EEG and HD-sEMG Acquisitions

G. L. Cerone, *Member, IEEE*, A. Giangrande, M. Ghislieri, *Member, IEEE*, M. Gazzoni, *Member, IEEE*, H. Piitulainen, and A. Botter, *Member, IEEE*

***Abstract*— Sensorimotor integration is the process through which the human brain plans the motor program execution according to external sources. Within this context, corticomuscular and corticokinematic coherence analyses are common methods to investigate the mechanism underlying the central control of muscle activation. This requires the synchronous acquisition of several physiological signals, including EEG and sEMG. Nevertheless, physical constraints of the current, mostly wired, technologies limit their application in dynamic and naturalistic contexts. In fact, although many efforts were made in the development of biomedical instrumentation for EEG and High Density-surface EMG (HD-sEMG) signal acquisition, the need for an integrated wireless system is emerging. We hereby describe the design and validation of a new fully wireless body sensor network for the integrated acquisition of EEG and HD-sEMG signals. This Body Sensor Network is composed of wireless bio-signal acquisition modules, named sensor units, and a set of synchronization modules used as a general-purpose system for time-locked recordings. The system was characterized in terms of accuracy of the synchronization and quality of the collected signals. An in-depth characterization of the entire system and an head-to-head comparison of the wireless EEG sensor unit with a wired benchmark EEG device were performed. The proposed device represents an advancement of the State-of-the-Art technology allowing the integrated acquisition of EEG and HD-sEMG signals for the study of sensorimotor integration.**

***Index Terms*— Biopotential acquisition systems, EEG, evoked potentials, High Density-surface EMG (HD-sEMG), sensorimotor integration, wireless body sensor network.**

Manuscript received June 15, 2021; revised September 8, 2021 and November 29, 2021; accepted December 2, 2021. Date of publication January 4, 2022; date of current version January 28, 2022. This work was supported by the University of Jyväskylä "Brain changes across the life-span" under Grant 311877. The work of H. Piitulainen was supported in part by the Academy of Finland under Grant 296240 and Grant 327288 and in part by the Jane and Aatos Erkko Foundation under Grant 602.274. *(G. L. Cerone and A. Giangrande contributed equally to this work.) (Corresponding author: G. L. Cerone.)*

This work involved human subjects or animals in its research. Approval of all ethical and experimental procedures and protocols was granted by the Ethics Committee of the University of Jyväskylä under Approval No. 369/13.00.04.00/2020, March 27, 2020.

G. L. Cerone, M. Gazzoni, and A. Botter are with the Laboratory for Engineering of the Neuromuscular System (LISiN) and the PoliToBIOMed Laboratory, Department of Electronics and Telecommunications, Politecnico di Torino, 10128 Turin, Italy (e-mail: giacintoluigi.cerone@polito.it).

A. Giangrande is with the Laboratory for Engineering of the Neuromuscular System (LISiN) and the PoliToBIOMed Laboratory, Department of Electronics and Telecommunications, Politecnico di Torino, 10129 Turin, Italy, and also with the Faculty of Sport and Health Sciences, University of Jyväskylä, 40014 Jyväskylä, Finland.

M. Ghislieri is with the Biolab and the PoliToBIOMed Laboratory, Department of Electronics and Telecommunications, Politecnico di Torino, 10129 Turin, Italy.

H. Piitulainen is with the Faculty of Sport and Health Sciences, University of Jyväskylä, 40014 Jyväskylä, Finland.

Digital Object Identifier 10.1109/TNSRE.2022.3140220

I. Introduction

IN EVERYDAY activities our body interacts with the ever-changing environment in smooth manner thanks to sensory feedback from the external environment (e.g. visual, auditory, tactile, etc.) and internal state of our body (e.g. proprioceptive) to the central nervous system. The brain is responsible for integrating these feedbacks with intentional motor planning to generate efficient motor output to the muscles [1]. The ability of the brain to properly combine external information to assist motor program execution is called sensorimotor integration [2]. The deterioration of this function due to ageing, traumatic events, or pathologies may lead to a wide range of motor impairments affecting the quality of life [3]–[5]. Although the neural control of movement in healthy and pathological individuals has been widely investigated during the last few decades, the way humans control their interactions with the environment remains one of the unsolved neuroscience research questions, because it often requires performing dynamic tasks in naturalistic conditions [6]. Corticomuscular (CMC) and corticokinematic (CKC) coherence analyses are widely used to study the cortical control of movement [1], [7]–[9]. The two methods require the simultaneous recording of brain activity using electroencephalography (EEG) or magnetoencephalography (MEG) simultaneously with muscular activities (EMG) in case of CMC or limb kinematics in case of CKC. Recently, High-Density surface EMG (HD-sEMG) has been used in CMC analysis [9], [10]. By recording EMG activity from multiple detection points over the muscle, HD-sEMG allows to describe the spatiotemporal pattern of the muscle activation and to extract relevant information on central and peripheral properties of the neuromuscular system such as the motor unit behavior (investigated through motor unit decomposition algorithms), [11]–[13].

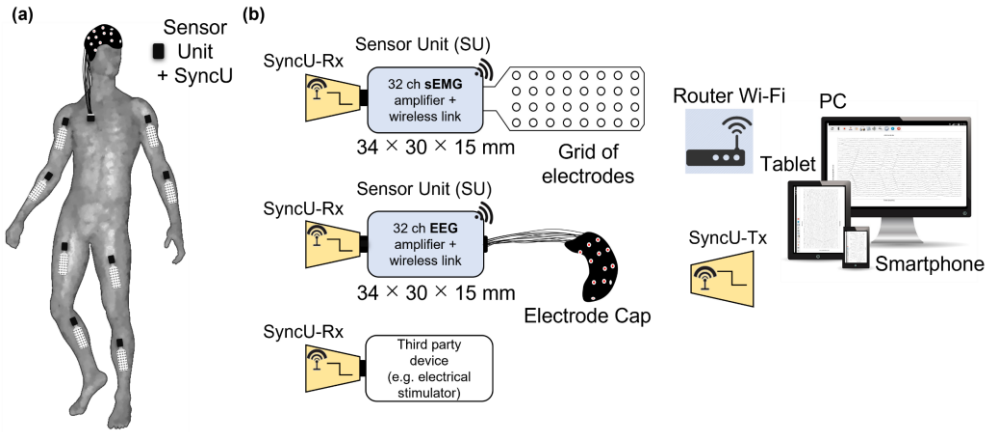

Fig. 1. System architecture. (a) Example of a wireless body sensor network composed of one EEG and 8 HD-sEMG sensor units. (b) From top to bottom: HD-sEMG sensor unit connected to a grid of electrodes, EEG sensor unit connected to an electrode cap, a third-party device (e.g., electrical stimulator, motion capture devices, force sensors). Each module is connected to the receiver module of a Synchronization unit (SyncU-Rx) receiving the wireless synchronization pulse from the transmitter (SyncU -Tx). Each sensor unit transmits the acquired signals to either a mobile device (smartphone or tablet with Wi-Fi connectivity) or a Personal Computer for real-time visualization and storage.

As compared to single-channel surface EMG, HD-sEMG provides a more accurate estimation of neural input issued to the muscle [11], [14], [15], thus improving the detected CMC [16]. Although all these techniques underwent significant advancements in the last 20 years, several bottlenecks limiting their integration and their concurrent application in naturalistic conditions outside the research lab still exist. One of the main issues concerns the physical constraints associated with the wired technology of the devices, which makes the experimental setups bulky, and thus unsuitable for dynamic/naturalistic tasks. Furthermore, wired acquisitions are usually more prone to interference and artifacts. To extend the usability and applicability of the devices towards naturalistic contexts, wireless devices for electrophysiological or biomechanical signal detection have been proposed [17], [18] and are now available on the market. However, these devices typically do not provide the possibility to readily integrate the acquisition of mixed signals (EMG, EEG, biomechanical variables) required to investigate sensorimotor integration. This leads to complex and unpractical setups often limiting the conditions in which data acquisition can be performed. It is not trivial to ensure the appropriate degree of synchronization between devices collecting different types of signals and not natively designed to be integrated with other, third-party devices (e.g., force transducers, inertial sensors, external trigger generators, transcranial magnetic stimulation device etc.). This is because standard wireless technologies based on high-throughput communication protocols (e.g., Bluetooth and Wi-Fi) cannot guarantee a sufficient degree of synchronization, often within one sample (i.e., few hundreds of μs), between data streamed by different transmitters without compromising the performances in terms of quality and affordability of the transmitted data. The emerging need for system integration requires modular systems natively conceived as part of an integrated wireless architecture but also sufficiently flexible to be synchronized with general-purpose, external devices. To the best of our knowledge, commercially available systems lack of all the requirements described before at the same time: wireless link, modularity, miniaturization, possibility to wirelessly synchronize each module with time delays within one sample, possibility to easily connect and integrate third-party instrumentation.

In this study, building upon the work described in [19], we developed a wireless system for the simultaneous and synchronous acquisition of HD-sEMG and EEG. Moreover, the system can interface with general-purpose instrumentation (third party devices, e.g., for real-time biofeedback or sensory multimodal stimulation providing, e.g., visual or auditory stimuli). Specifically, we hereby: (i) present the overall system architecture and the main design choices related to the HD-sEMG/EEG acquisition module, (ii) describe the design of the synchronization system for time-locked recordings, (iii) validate the performances of the wireless EEG device using a conventional wired EEG system as a benchmark, (iv) show a use-case validation study.

II. Hardware Design and Prototyping

A. System Architecture

The proposed system implements a client-server wireless Body Sensor Network (wBSN) (Fig. 1) composed of a set of Sensor Units (SU, clients) for the acquisition of HD-sEMG or EEG signals and one device (server) for signal visualization and storage. A synchronization system allows the synchronization of signals coming from different SUs. The entire set of sensors and the connected synchronization modules constitutes a wireless Body Sensor Network (wBSN).

Each SU has 32 analog and one digital input. The SUs perform the input signals conditioning, sampling and transmission to the receiver (a mobile device or a personal computer) through a Wi-Fi access point acting as a router for real-time visualization and storage.

The synchronization system is composed of a set of modules (SyncU) communicating over a dedicated, low-latency radio channel. One SyncU is configured as transmitter (SyncU-Tx) while the others are configured as receivers (SyncU-Rx) and connected to the SUs that must be synchronized. The

SyncU-Tx transmits a synchronization signal. The signal received by the SyncU-Rx is sampled throughout the SU digital input and transmitted to the wBSN server. The choice of designing an external synchronization module instead of integrating it into the SU module allows to: (i) reduce the size of the SUs when no synchronization is needed (e.g. when a single HD-sEMG or EEG SU is used), (ii) use a single, configurable, SyncU either as receiver and transmitter, (iii) provide the synchronization signal to any device with a digital input available (e.g., footswitches, auditory stimuli used to provide EP response, etc.), thus enabling the possibility to extend the wBSN with external, third-party instrumentation. Furthermore, using an external synchronization device reduces the total cost of the system as the same system can be used for both the SU and third-party devices. However, future developments requiring a higher degree of miniaturization of the whole system could integrate both the sensor and synchronization units into a single device. Apparently similar synchronization systems are commercially available (e.g. SyncSE, OT Bioelettronica, Italy) but they have a time latency above one sample (33.2 ms) that may not be adequate for studying short-latencies responses. Other open-source software synchronization systems [20], [21] are based on timestamp recording, which makes them unsuitable for real time applications as they require offline post processing.

TABLE I
TECHNICAL SPECIFICATIONS OF THE SYSTEM

Description	Parameter	Value
Num. of analog channels	N_A	32
Num. of digital channels	N_D	1
Bandwidth (EMG mode)	BW_{EMG}	10 Hz – 500 Hz
Bandwidth (EEG mode)	BW_{EEG}	0.1 Hz – 500 Hz
Gain	G	192 ± 1 V/V
Common Mode Rejection Ratio	CMRR	82 dB
Input Impedance module	$\lvert Z_{In}\rvert$	1.3 GΩ (10 Hz) 13 MΩ (1 kHz)
Input Range	IR	10 mV_{pp}
RTI Noise	N_{RTI}	$< 3\ \mu V_{RMS}$
A/D Resolution	Res	16 bit
Sampling Frequency	f_s	2048 sps
Communication	-------	Wi-Fi
Receiver Type	-------	PC, Smartphone or Tablet
Max. Sync. delay	Δt_{Sync}	±5 µs
Max. time latency	Δt_{Lat}	±400 µs
Max. TX distance	d_{TX}	22 m (<0.02% data loss)
Power Supply	-------	200 mAh 1-Cell LiPo Battery
Life time (transmitting)	T_{TX}	3h
Dimensions	-------	3.4 cm × 3 cm × 1.5 cm
Weight	-------	16.7 g

B. Hardware Design and Bench Characterization

1) Sensor Unit: The SU design was based on the design of the HD-sEMG SU described in [19]. The SU consists of three main building blocks:

i. The Bio-signals Acquisition Unit implementing the conditioning and quantization of 32 EMG/EEG signals at 2048 sps with 16 bit resolution;
ii. The Control Unit implementing the sampling and wireless transmission of the collected signals through a 2.4 GHz Wi-Fi link;
iii. The Power Management Unit providing a regulated 3.3 V power supply and handling the wireless battery charging.

The SU is powered through a 600 mAh single-Cell LiPo Battery. The detection systems (grid of electrodes for HD-sEMG or EEG caps) connect to the SU analog inputs through a ZIF connector (Molex 54104-3231, Illinois, USA). The RHD2132 chip [22] (Intan Technologies, California, USA) was selected for both the HD-sEMG and EEG analog front-end because of the following main characteristics: (i) compact size (9 mm × 9 mm, QFN package), (ii) low-power, 32 monopolar AC-coupled analog front-ends with fixed gain (192 V/V), (iii) programmable bandwidth (0.1 Hz - 20 kHz) compatible with both EEG and sEMG signals, (iv) availability of non-conditioned auxiliary channels for synchronization, and (v) availability as pre-packaged component for standard pick and place mounting of the PCB.

Table I shows the main features of the HD-sEMG and EEG SUs. With respect to the SU described in [19], the SU herein designed:

i. implements a mixed-signal bipotential acquisition system, sampling and transmitting 32 analog signals and one auxiliary digital signal (used to acquire the synchronization signal received by the SyncU-Rx modules).
ii. allows to dynamically select the bandwidth of the analog front-end during the SU startup to adapt to the acquisition of both EEG (0.1 Hz - 500 Hz) and HD-sEMG (10 Hz – 500 Hz) signals.

2) Synchronization Unit: A multi-function wireless synchronization module has been designed and prototyped. We chose to develop a single module for both transmission (SyncU-Tx) and receiver operations (SyncU-Rx) to simplify the design and reduce costs.

The transmitter is powered through a cable by a common USB phone charger containing a 3.3 V step-down DC/DC converter (LM3671MF-3.3, Texas Instruments, USA) and it is equipped with a configuration button that allows selecting the synchronization pulse transmission mode between (i) *automatic*: a programmable pulse train (e.g., 100 ms long pulse with 2 s period) is internally generated and transmitted, (ii) *external*: a synchronization signal generated by an external device (e.g., a push button, a footswitch, a signal generator, or a third-party device that acts as a synchronization/trigger signal source) is acquired and transmitted. The synchronization pulses are transmitted in broadcasting mode to all the SyncU-Rx modules. A 2.5 mm audio jack (50-00407, Tensility Int. Corp. USA) allows, when connected to the SU, to power the module and communicate the received synchronization pulse to the SU. When the SyncU-Rx receives the synchronization pulse, it generates a digital signal that can be acquired by any system connected to it via the 2.5 mm audio

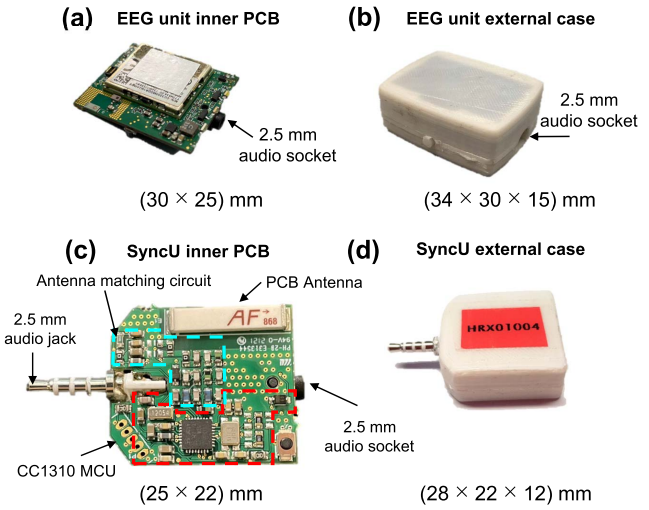

Fig. 2. Acquisition and Synchronization modules. (a) and (c) show the top view of the inner PCB with mounted components respectively for the EEG sensor unit (SU) and the synchronization unit (SyncU) with its main blocks. The PCB dimensions are: (a) 30mm × 25mm and (c) 25mm × 22mm. (b) and (d) show respectively the EEG SU and the SyncU in a 3D printed PLA case leading to a total encumbrance of (b) 34mm × 30mm × 15mm and (d) 28mm × 24mm × 12mm.

jack. A 2.5 mm audio socket (SJ2-25964A-SMT-TR, CUI Device, USA) positioned on the opposite side of the jack connector (Fig. 2a) is used for the connection to the external generator in *external mode*. The SyncU design was kept as simple as possible, minimizing the number, size, and cost of the components. The SyncU consists of two main hardware blocks: i) the wireless MCU, managing the wireless transmission/reception of synchronization pulses, and ii) the antenna matching circuit, used to effectively transmit wireless signals. The CC1310 wireless MCU (Texas Instruments, USA) [23] was selected as transceiver to implement a low-latency radio channel characterized by excellent performance of the receiver in terms of sensitivity (-124 dBm) and selectivity (56 dB) and a transmission carrier frequency of 868 MHz. The CC1310 wireless MCU implements a proprietary wireless protocol based on an IEEE 802.15.4 physical layer (the same as the ZigBee wireless protocol) that allows building a Personal Area Network (PAN) with a low power consumption of about 15 mW during signal reception. The adoption of a wireless protocol different from that used for the SU communication (Wi-Fi) [19] was motivated by the need of guaranteeing the required performance in terms of synchronization delays and latencies between different SyncU modules. Therefore, the system architecture relies on two different communication protocols used for SUs-receiver data exchange (Wi-Fi, characterized in [19]), and SUs synchronization through the SyncU modules (IEEE 802.15.4). The ANT-868-CHP-T (Linx Technologies, USA) 868 MHz ceramic chip antenna was selected and the antenna's impedance matching circuit was designed accordingly to the LAUNCHXL-CC1310 reference design (Texas Instruments, USA).

3) Prototyping: Commercially available Off-The-Shelf (COTS) components were used for the design of SyncU PCB. The minimization of the system's encumbrance was one of the primary objectives of the design. The SU PCB (Fig. 2a) consists of an eight-layers, 1 mm thick PCB (dimensions: 3.0 cm × 2.5 cm), and was encapsulated into a 3D-printed (Fig. 2b) case [19]. Fig. 2c shows the SyncU PCB. It consists of a two-layers, 0.8 mm thick PCB (dimensions: 2.5 cm × 2.2 cm) with components mounted on both sides. Fig. 2d shows the SyncU final prototype encapsulated in a 3D-printed plastic case. The total encumbrance of the SyncU module resulted in 2.8 cm × 2.4 cm × 1.2 cm (thickness). Two EMG/EEG SUs and four SyncU modules were built and prototyped.

4) Bench Characterization: The bench characterization of the system was mainly focused on the synchronization performances and the test of the EEG SU analog front-end since the HD-sEMG SU was previously characterized in [19]. The reader is redirected to [19] for a complete characterization of the SU module.

a) EEG SU: The input-referred noise level of the front-end amplifier was measured by shorting and connecting to the reference pin the analog inputs of the RHD2132 chip and calculating the RMS voltage for each channel over a 30 s long epoch of signal. The mean noise level across channels was $2\,\mu V_{RMS} \pm 0.2\,\mu V_{RMS}$. The band-pass gain of each channel was measured by applying a 40 Hz, 2 mV_{pp} sinewave to the input of the RHD2132 front-end and calculating the ratio between the output and the input peak-to-peak amplitude. The bandwidth of each monopolar front-end was measured by applying a 2 mV_{pp} sinewave to the input of the EEG SU and varying, for each channel, the input frequency to find the -3 dB attenuation with respect to the amplifier's nominal gain. The measured in-band gain for each channel was 192 V/V ± 1 V/V (CoV= 0.5%) within a 0.1 Hz - 500 Hz frequency band. The measured inter-channel gain variability was between 0.5% and 1% and results comparable with that observed in [19]. The minimum input voltage range was 10 mV_{pp} (± 5 mV_{pp}) across all the analog acquisition channels. The total harmonic distortion was calculated in the 0.1 Hz - 100 Hz frequency band for three sinusoids of different amplitude (2 mV_{pp}, 4 mV_{pp}, and 8 mV_{pp}) and resulted less than 0.8%, in agreement with the values reported in the RHD2132 datasheet [24]. The total harmonic distortion was lower than 0.36% in mid-band frequencies (20 Hz and 80 Hz). The robustness of the EEG SU to the second-order non linearities of the RHD2132 front-end amplifier (Intan Technologies, USA) was evaluated by computing the first-order IMD products. A linear combination of two similar tones (amplitude 8 mV_{pp}, $f_1 = 39$ Hz and $f_2 = 41$ Hz) was applied to the inputs of the EEG SU through an analog mixer circuit. The first order IMD products, located at 37 Hz and 43 Hz, resulted in a 135.5 dB ± 6.0 dB attenuation with respect to the input signals.

b) SyncU bench characterization: Four SyncU modules (1 SyncU-Tx and 3 SyncU-Rx) were characterized in terms of power consumption and wireless performance. The SyncU-Tx was powered through a 5 V USB phone charger and the measured power consumption during the trigger signal transmission was 32.5 mW (6.5 mA current consumption). The measured power consumption of the SyncU-Rx module was

21.45 mW (6.5 mA current consumption). The higher power consumption of the SyncU-Tx module is not critical as it is intended to be used connected to a power line source or a USB port and not to a battery-powered device (as opposed to SyncU-Rx that is connected to a SU). The wireless performances of the synchronization unit were characterized by measuring the latency between transmitted and received signals and the time delay between the signal received by different SU modules. The SyncU-Tx module was configured in *automatic mode*. The output of all the SyncUs was acquired through a mixed-signal oscilloscope (MSO-X-2024A, Keysight Technologies, USA). We observed an average time latency of 400 μs, with a maximum delay between receivers of 5 μs. Considering that most of the HD-sEMG/EEG signal acquisition systems have a sampling frequency lower than 2 kHz (500 μs period), our synchronization system enables applications requiring latencies below one sample.

III. Experimental Validation

A. Material and Methods

Evaluating new devices and technologies by on-field experimental tests is of paramount importance dealing with the design and development of biomedical instrumentation. Although bench characterization allowed us to deterministically quantify the compliance of our device with the proposed technical specifications, the actual experimental use includes several variables (e.g., patient's capacitive coupling to the power line [25]–[27], electrode-skin impedance unbalance [26], [28] etc.) which are difficult to estimate. Hence, we performed a head-to-head (i.e. on the same subject, day, condition) quantitative comparison with a commercially available EEG system because the EEG signal features and the interference/noise levels affecting bio-signals depend on factors that may change substantially when recordings are performed in different labs/sessions. Four experimental protocols were designed to validate the on-field performances of our system in terms of quality of detected signals, inter-module synchronization, and synchronization with external devices. All tests were performed with our system (Device Under Test - DUT) and with a Benchmark Device (BD). The selected BD was Bittium (NeurOne Tesla, Oulu, Finland) because: (i) it is a commercially available medical device, (ii) it is a good test-bench for our wireless synchronization, due to its wired link which ensures negligible latencies, (iii) it is fully integrated with standard software for sensory stimulations. EEG signals were collected using three different but commonly used sensory stimulation designs in the field of EEG: auditory, visual, and somatosensory stimulations. The aim was to validate the wireless EEG module through the comparison of DUT vs. BD in the shape (timing and amplitude) and in the topographic distribution of the respective evoked cortical EEG responses. The DUT *versus* BD comparison of the cortical responses latencies during sensory stimulations was used to experimentally verify the possibility to synchronize the EEG SU with third-party devices used to provide the stimulation patterns. The fourth experiment represents an active task to quantify the corticospinal coupling between coherent cortical (EEG) and muscular (HD-sEMG) activities: a protocol to compute CMC. EEG, HD-sEMG, and an external signal (force) were collected simultaneously to verify the concurrent and synchronous wireless acquisition of multiple biological signals in this relevant experimental context. The details of the four validation tests are reported in the following sections.

1) Participants: A group of ten healthy subjects (6 males, 4 females, age range: 24–40 yrs) was recruited for the experimental validation of the designed system. All the participants were right-handed (mean score range 92.37 on a scale from –100 to 100, according to the Edinburgh handedness inventory [29]). Participants did not report any neurological or motor disorder. The study was approved by the Ethics Committee of the University of Jyväskylä before starting the measurements (approval number: 369/13.00.04.00/2020). The study was conducted in accordance with the Declaration of Helsinki and written informed consent was obtained from all participants after having provided them with a detailed explanation of the study procedure itself.

2) Validation Protocols: The four experiments (auditory, visual, and somatosensory stimulations and active isometric contraction for CMC) were carried out in the EEG Laboratory in the Department of Psychology, University of Jyväskylä (Jyväskylä, Finland).

Scalp signals were recorded during all four experiments with a 30 head-mounted electrodes cap (EasyCap GmbH, Gliching, Germany) kept in place between consecutive tasks (for BD-DUT comparison). The Ag/AgCl electrodes embedded into the cap were in accordance with the international 10-20 system. An abrasive paste (NuPrep, Weaver and Company, Aurora, USA) was used to gently scrab each electrode site with a cotton swab after having placed the cap on the scalp. Every cavity was then filled with a conductive gel (NeurGel, SPES MEDICA, Genova, Italy). In addition, EOG was recorded with two electrodes (30 mm $\times$ 22 mm Ambu s.r.l., Denmark) placed in the up-left and down-right corners to detect and further remove eye movements and blinks. EEG signals were referenced to the FCz electrode of the cap for both devices.

A detailed description of the four experimental protocols is reported hereafter.

a) Auditory stimulation: Acoustic tones (1 kHz, 60 dB, 100 ms duration including 10-ms rise and fall ramps) were presented alternatively to the right and left ear of the subjects through shielded earphones (ER-3C, 50 Ohm, Etymotic Research). In the meanwhile, participants were asked to gaze at a fixation cross showed on a screen in front of them. Tones were randomly delivered to the left and the right earphone every 2 s with a random jitter of $\pm$ 250 ms [30]. One hundred stimuli per ear were delivered to each participant. (Fig. 3a). The stimulation pattern was programmed using the stimulus delivery software Presentation (Neurobehavioral Systems, Berkeley, CA). This experiment required an EEG SU and two SyncU modules. A SyncU-Tx module was configured to acquire an external signal for each stimulus (driven by the software) and to transmit it to the SyncU-Rx.

b) Visual stimulation: Flashes of a black-and-white checkerboard pattern (14.6 deg $\times$ 8.2 deg, check size

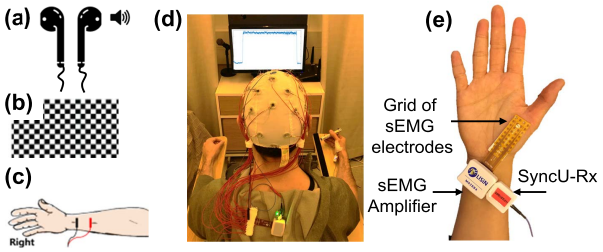

Fig. 3. Experimental protocol and setup. (a) Auditory stimulation; (b) Visual stimulation; (c) Electrical stimulation of the median nerve. (d) Isometric contraction task: visual force feedback during isometric pinch grip of the right hand at 10% of MVC for 4 minutes; (e) Experimental setup during the isometric contraction: high-density surface electromyography grid (8 × 4 electrodes, inter-electrode distance: 5 mm), wireless HD-sEMG amplifier and SyncU-Rx modules.

0.7 deg × 0.7 deg) were presented on a screen placed at 1.5 m in front of the subjects every 2 s with a random jitter of ± 250 ms (100 stimuli, duration 100 ms) [30]. (Fig. 3b). One EEG SU was connected to a SyncU-Rx module. The visual stimulation pattern was provided through a screen controlled by the Presentation software. The same software was used to deliver a synchronization pulse to the SyncU-Tx at the start of each stimulus.

c) Somatosensory stimulation: The right median nerve was electrically stimulated using two surface electrodes (30 mm × 22 mm, Ambu s.r.l., Denmark) placed 2 cm proximal to the wrist according to the course of the nerve, 1 cm apart. A neuromuscular electrical stimulator (DS7AH, Digitimer Ltd, UK) was used to deliver 0.2 ms long constant current monophasic pulses. The pulse intensity was adjusted according to the participants' motor threshold, defined as the lowest current level inducing a visible mechanical response of the thumb (I = 8.5 mA ± 2.1 mA, mean ± SD across participants). One hundred stimuli were delivered every 2 s with a random jitter of ± 250 ms [30] (Fig. 3c). The wBSN included an EEG SU and a SyncU-Rx. The electrical stimulator was used as a third-party device and connected to a SyncU-Tx.

d) Isometric contraction for CMC: This experiment was included to demonstrate the feasibility and straightforward configuration of a hybrid EEG/HD-sEMG recordings synchronous wBSN through the proposed system. Participants were seated with their right hand on the armrest of the chair, maintaining a steady isometric pinch contraction by the thumb and index fingers (flexion) on a force transducer (FS 6 N - model 1004; Vishay Precision Group, Malvern, PA). Before EEG recordings, subjects performed a maximum voluntary contraction (MVC) test lasting 3–4 s. A rigid load cell (FS 30 N - model 1042, Vishay Precision Group, Malvern, PA) was used to measure the MVC during the same pinch task. Participants were then asked to maintain a constant force level at 10% ± 2% of their MVC for 4 minutes. A visual, real-time force feedback (Fig. 3d) was provided on the screen in front of them. Force signals were sampled at 1 kHz and stored using a data acquisition unit (Micro1401-4, Cambridge, England, UK). The wBSN used during the motor task included one EEG SU, one HD-sEMG SU, and two SyncU-Rx modules connected to each SU. The data acquisition unit was used as a third-party device to synchronously record EEG, HD-sEMG, and force signals. EMG activity from the right flexor pollicis brevis muscle was collected using a grid of 32 Ag/AgCl electrodes (4 rows by 8 columns, inter-electrode distance (IED) of 10 mm - LISiN, Politecnico di Torino, Torino, Italy). The skin was gently scrubbed with an abrasive paste (Nuprep, Weaver and Company, Aurora, USA) and the grid was attached to the skin with the columns aligned according to the fibers orientation of the right thenar muscles [9]. Monopolar HD-sEMG signals were detected, conditioned (Bandwidth 10 Hz – 500 Hz, Gain 46 dB), and sampled at 2048 Hz with 16-bit resolution through the HD-sEMG SU [19].

3) Data Analysis: Time and frequency domain variables were analyzed to compare the quality of EEG signals detected by our system and by the BD and to assess the feasibility of an integrated detection of EEG/HD-sEMG measurements using our system. Specifically, the amount of Power Line Interference (PLI) during experimental conditions and the distribution of power across different EEG frequency bands were evaluated. Event-Related Potentials (ERP) and CMC provided information about the spatiotemporal alignment of the synchronized EEG/HD-sEMG recordings. All the analyses were performed offline using the Matlab Software (Mathwork Inc, Natick, MA, USA).

a) Power spectral density: The Power Spectral Density (PSD) of EEG signals acquired during the isometric contraction (0.5 Hz – 60 Hz) was computed using a non-overlapped flattop window over a 30-s window. Relative EEG power of the signals recorded with the BD and the DUT was separately computed for different frequency bands (Delta 0.5 Hz – 4 Hz, Theta 4 Hz – 8 Hz, Alpha 8 Hz – 14 Hz, Beta-1 14 Hz – 21 Hz, Beta-2 21 Hz – 30 Hz, Gamma 30 Hz – 45 Hz) normalized with the total absolute EEG power (0.5 Hz – 45 Hz). The median band power of all the 30 EEG channels was extracted for each participant, separately for each frequency band. The comparison between the DUT and BD was then performed evaluating the mean and standard deviation of the band power in each frequency band across participants.

b) Power line interference and signal to interference ratio: The power line contribution to the detected EEG signals was estimated computing the RMS value of the 50 Hz component and the Signal-to-Interference Ratio (SIR) of the collected signals. Estimations were performed on a 3-min long epoch of filtered EEG signals (4^{th} order Butterworth, bandpass filter 0.5 Hz – 60 Hz) collected during the isometric contraction task. The RMS value of the 50-Hz contribution to the detected signals was computed by filtering, for each channel, the raw EEG signals with a 48 Hz – 52 Hz bandpass filter (4^{th} order Butterworth filter). The median RMS value across all EEG channels (n = 30) was extracted for each participant. The mean and standard deviation across all participants (n = 10) was then used as a measure of comparison between the BD and the DUT. For each subject, the SIR was calculated according to (1). The EEG variance (σ_{sig}) was used to estimate the power of the collected signals without interference (Notch filter at 50 Hz, 4^{th} order Butterworth band-stop filter) across

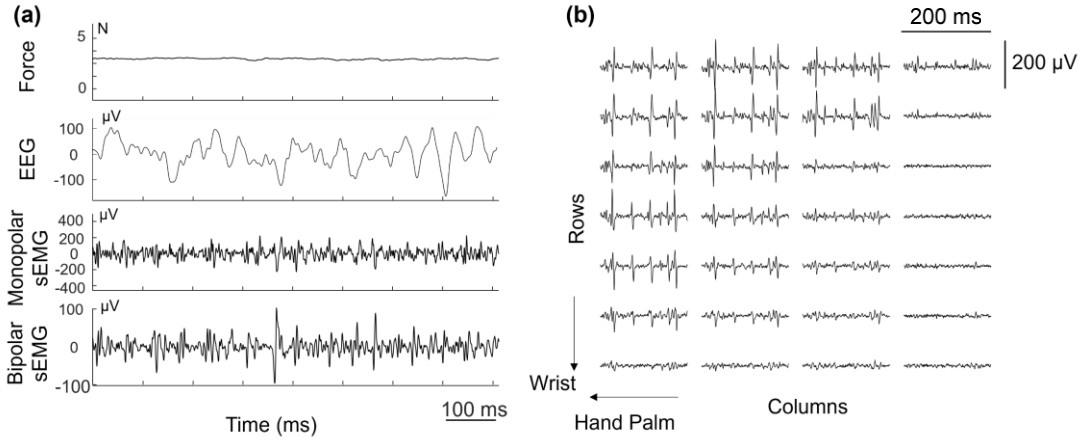

Fig. 4. (a) Examples of measured signals during the isometric contraction task of a single subject (800-ms epoch). From top to bottom: 10-Hz low-pass filtered force signal (10% of maximum voluntary contraction), wireless EEG signal (channel C3), one monopolar and one bipolar EMG signal (passband 20 Hz – 400 Hz). The selected EMG and EEG signals are those showing the highest peak of corticomuscular coherence. (b) Single differential HD-sEMG signals of a representative participant during a 200 ms epoch of the isometric contraction task. Firings of individual motor units are clearly visible.

channels. The EEG spectral components in the 48 Hz – 52 Hz band were considered negligible with respect to the total signal power. Mean and standard deviations were calculated from the variability across participants to compare the performances of standard and wireless EEG recording systems.

$$SIR = 20log\frac{\sigma_{sig}}{RMS_{int}} \quad (1)$$

c) EEG preprocessing: EEG noisy channels, due e.g. to a bad electrode-skin contact, etc., were identified by visual inspection and replaced with the average of all their neighboring channels by using FieldTrip Matlab toolbox for both the BD and the DUT. [31]. On average, 2 channels out of 30 were replaced among all the participants. The EEG signals were spatially filtered using the average reference of all EEG channels for further analyses. Independent Component Analysis using FieldTrip Matlab toolbox was used to separate the EEG components and reject the ones related to the eye blink artifacts chosen as those matching the EOG pattern (i.e., showing the highest correlation with the EOG) recorded time-locked with the EEG [32].

d) EEG event-related potential (ERP) computation: For each stimulation type (i.e., auditory, visual, and somatosensory), the EEG signals were averaged with respect to the stimulus onsets for 700-ms epoch (from –100 to 600 ms) to obtain the ERPs for each EEG channel separately. Three regions of interest (ROI) were identified from the 30 EEG channels depending on the stimulus type. The ROI included (contralateral to the stimulated right hand) motor cortex (C3, T7, FC5, CP5) for the auditory, visual, and somatosensory stimulations, respectively. The EEG responses of the ROI were then averaged for each participant and stimulation type separately. Finally, the ERPs were grand averaged across all participants. Peak latencies and amplitudes were extracted by considering the common ERP components specific for each sensory domain (i.e., auditory N100-P100, visual N100-P200, somatosensory N20-P30) [30], [33], [34]. EEG electrodes located in the auditory cortex (left: T7, TP9; right: T8, TP10), the visual cortex (O1, O2, Iz), the left (contralateral to the stimulated right hand) motor cortex (C3, T7, FC5, CP5) for the auditory, visual, and somatosensory stimulations, respectively. The EEG responses of the ROI were then averaged for each participant and stimulation type separately. Finally, the ERPs were grand averaged across all participants. Peak latencies and amplitudes were extracted by considering the common ERP components specific for each sensory domain (i.e., auditory N100-P100, visual N100-P200, somatosensory N20-P30) [30], [33], [34].

e) Corticomuscular coherence (CMC) computation: HD-sEMG signals were offline bandpass filtered (20 Hz – 400 Hz) [35]. Single Differential signals were first derived from the monopolar ones along the four columns of the EMG electrode grid. The location of the innervation zone (IZ) was identified, by visual inspection, as the single differential channel showing the lowest amplitude and inversion of the signal polarity with respect to its proximal either distal neighbors [36]. Then, the monopolar signals located over the IZ (i.e. showing the highest monopolar signal amplitude) were used to compute the CMC [9]. Fig. 4a and Fig. 4b show examples of the measured signals of a presentative participant performing the isometric contraction task. HD-sEMG and EEG signals were divided into 512 ms long epochs with 400 ms epoch overlap. The corresponding spectral resolution was 2 Hz. This spectral resolution has been used by many experiments as a good compromise between time and frequency resolution [8], [37], [38], ensuring sufficient number of epochs in the CMC analysis and capturing the coherent physiological event (bandwidth of ∼10–15 Hz). EEG epochs exceeding 200 mV were rejected to avoid contamination of the EEG data by eye movements, muscle activity, and other artifacts. Power spectra were calculated between EEG and unrectified, RMS-normalized sEMG signals [39]. The coherence spectra between EEG signals (30 channels) and the sEMG pair previously identified were computed according to Halliday *et al.*, 1995 [40]. The chosen coupling measure was the magnitude of the squared coherence

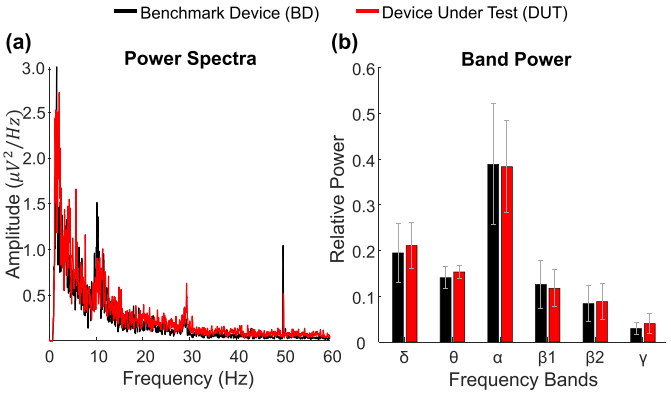

Fig. 5. (a) Power spectral densities of a channel (C3) of signals recorded with the benchmark device (BD - black color) and the device under test (DUT - red color) of a subject performing the isometric contraction task. (b) Mean values of relative band power at each band for the benchmark device (BD - black color) and the device under test (DUT - red color) normalized with respect to the total absolute power in the frequency band 0.5 Hz – 45 Hz. Error bars indicate the variability (standard deviation) across channels subjects (n = 10) during the isometric contraction. (Wilcoxon signed rank test showed no significant differences between the two systems for all frequency bands).

as previously done in similar studies [9], [41], [42]. CMC strength was defined as the maximum coherence value in the 10 Hz – 30 Hz frequency band across the midline and contralateral channels to the side involved in the task (i.e. Nc = 20). Furthermore, scalp topographies were obtained by means of the computation of the root mean square value over the frequency bands of interest (alpha 8 Hz – 14 Hz, beta 13 Hz – 30 Hz, gamma 30 Hz – 45 Hz). The CMC RMS values were interpolated to a standardized 30-channels electrode layout to visualize the topographic distributions of CMC across the scalp EEG electrodes.

4) Statistical Analysis: A Wilcoxon signed rank test was used to examine differences between the EEG recording systems (BD and DUT) on the following features: EEG power at specific frequency bands, SIR, primary ERP components amplitude and latency. The choice of carrying out non-parametric statistical tests was determined by the limited number of participants and the non-normal distribution of the considered variables (Shapiro-Wilk statistical test). Spearman correlation coefficients were computed across the participants to judge the agreement in the quantified ERP features between the EEG recording systems (BD and DUT). The statistical significance of individual CMC (peak value across the EEG signals of interest) was assessed under the hypothesis of linear independence of Fourier coefficients from epoch to epoch at each frequency of interest, taking into account the use of overlapping epochs [40], [43]. The α-level was set to 0.05/Nc, where Nc = 20 (number of midline and contralateral channels to the side involved in the task) was chosen to correct for multiple comparisons among subjects.

B. Results and Discussion

1) Power Spectral Density: Fig. 5a shows the PSD of the C3 electrode of EEG signals collected through the BD and DUT. The EEG signal power is mainly concentrated at physiological frequency ranges, predominantly in the 0.5 Hz – 30 Hz band. Fig. 5b shows that both devices detect an expected prominent alpha rhythm that is the most dominant rhythmic activity in the human brain [17] even during active isometric task and in the primary motor cortex. No statistically significant differences were observed in the relative mean EEG power between the EEG systems in any of the bands ($p > 0.54$ across the bands).

2) EEG Signal Interference: The RMS of powerline interference at 48 Hz – 52 Hz band did not differ significantly between the BD and the DUT (1.70 μV $\pm$ 0.31 μV vs. 1.47 μV $\pm$ 0.46 μV (mean $\pm$ SD across participants, $p = 0.28$ Wilcoxon rank-sum statistical test). These RMS values are comparable to the noise floor of the device, demonstrating the good performance of the EEG SU in terms of rejection of power line interference. Similarly, no significant effect of the recording system was found on the SIR of the BD and the DUT (25.40 dB $\pm$ 3.26 dB vs. 29.76 dB $\pm$ 6.22 dB, (mean $\pm$ SD across participants, $p = 0.15$, Wilcoxon signed-rank statistical test). Therefore, we conclude that the 50-Hz component of the power line interface affected similarly the quality of both the EEG recordings in the experimental conditions considered. This evidence is particularly important given the high relevance of PLI-related problems in biopotential recordings [25], [44], [45]. Although several hardware and signal processing techniques aimed to remove power line interference were proposed in the last twenty years [46]–[48], it is required to design biopotential amplifiers with high PLI rejection to avoid saturation at the input/output of the amplifier and improve the overall SNR of the collected signals [15], [49].

3) ERP to Sensory Stimulations: Fig. 6a shows the grand average of auditory, visual and somatosensory ERPs recorded with the two devices. ERPs components were similar for both EEG systems in each stimulation modality (Spearman correlation coefficients: auditory $r = 0.89 \pm 0.03$, visual $r = 0.96 \pm 0.01$ and somatosensory $r = 0.85 \pm 0.09$; mean $\pm$ SD across participants). Table II reports a summary of ERP latencies and amplitudes. No significant changes were observed between the two recording systems for both ERP variables ($p > 0.38$ for ERP latencies and $p > 0.08$ for ERP amplitudes across the sensory stimulations). Results suggest that the two recording systems provide the same amount of spatiotemporal information under the same type of stimulation, consistently with previous ERP studies [30], [33], [34]. A high intra- and inter-individual reproducibility of the evoked responses was observed for auditory and visual stimulations. Somatosensory ERPs showed higher intra- and inter-subject variability, but it was not atypical. Despite the observed variability, we were able to detect reproducibly the typical short-latency components (i.e., N20 and P30, see Table II). Moreover, the degree of intra- and inter-subject variability shown by the standard deviation of the grand average ERPs of Fig. 6a was similar between the two EEG systems, indicating that there was no relevant effect of the used device. The source of this variability could be associated with different factors. In fact, the somatosensory responses are typically more variable across individuals due to a higher degree of anatomical and functional variations in the sensorimotor cortices compared to the visual and auditory ones. Another factor is that the electrical stimulation is more difficult to perform and standardize across the participants

TABLE II
PEAK LATENCIES AND AMPLITUDES (MEAN ± SD) OF SENSORY STIMULATIONS ERPS

Stimulation Type	ERP Component	Peak Latencies (ms)			Peak Amplitudes (μV)		
		BD	DUT	p(*)	BD	DUT	p(*)
Auditory	P100	90.70 ± 6.82	86.13± 10.73	0.38	7.86 ± 2.99	7.22 ± 3.17	0.62
	N170	179.75 ± 38.01	173.92 ± 29.55	0.91	5.98 ± 2.88	6.57 ± 3.29	0.68
Visual	N100	113.20 ± 16.52	116.43 ± 10.21	0.62	15.79 ± 7.14	14.20 ± 7.51	0.62
	P200	192.55 ± 15.61	191.85 ± 17.99	0.85	15.97 ± 6.87	14.50 ± 7.03	0.52
Somatosensory	N20	12.85 ± 10.59	16.06 ± 9.74	0.42	0.97 ± 0.72	0.98 ± 0.85	0.16
	P30	36.55 ± 13.92	38.33 ± 14.63	0.71	4.37 ± 1.95	3.06 ± 1.40	0.08

(*) Wilcoxon signed rank test.

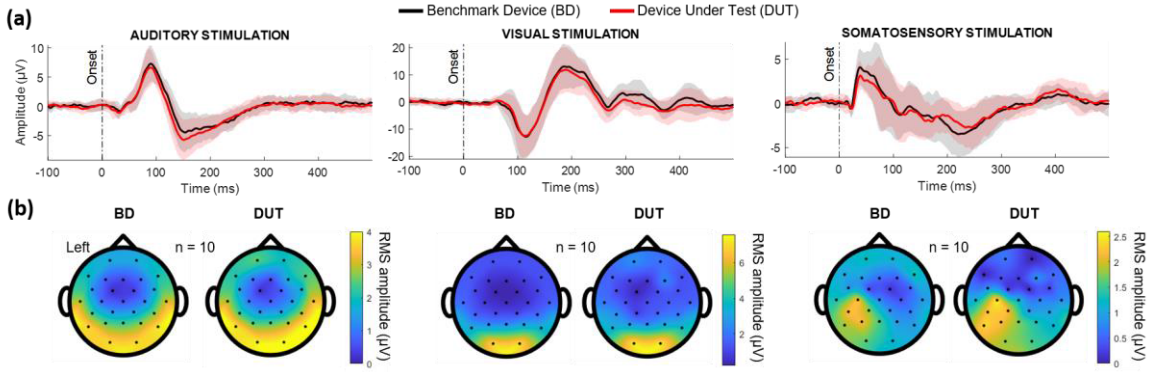

Fig. 6. Grand averages (a) ERPs and (b) scalp topographies across all subjects (n = 10) during conventional stimulations – from left to right: auditory, visual and somatosensory stimulation. (a) ERPs were recorded through the benchmark device (BD - black traces) and the device under test (DUT - red traces). Only a subgroup of channels was averaged for each subject over 600-ms epochs, according to the scalp region involved in the response to the stimulations. The shaded intervals indicate the standard deviations over all the subjects. From top to bottom: auditory, visual and somatosensory responses. (b) Topographies of the averaged visual responses (n = 100 stimuli) recorded with both devices (BD and DUT) (rms values of EEG signals on a 250 ms-window after the stimulus).

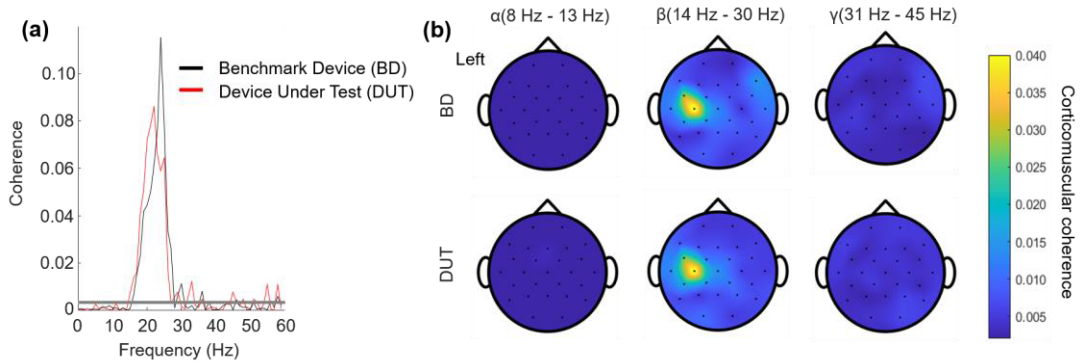

Fig. 7. CMC results from a representative participant. (a) Coherence spectra between sEMG and EEG (most coherent EEG channel: C3). Gray horizontal line indicates the threshold for statistical significance ($p < 0.05$). Black traces (BD) and red traces (DUT) are superimposed. (b) EEG/EMG coherence scalp topographies at alpha, beta and gamma bands (from left to right). On the upper panel topographies obtained from the benchmark device recordings, on the lower panel topographies obtained from the device under test recordings.

(e.g., in terms of definition of the stimulus intensity and/or electrode placement on the wrist).

4) Corticomuscular Coherence (CMC): All participants completed the flexion of the thumb at the requested force level (3.91 N ± 1.95 N) without reporting discomfort or perceptible fatigue. Three out of 10 participants showed significant CMC in the beta rhythm with both devices. This result was not atypical. In fact, even under magnetoencephalographic studies (usually the preferred technology dealing with coherence analysis) weak CMC strength, sometimes lower than the significance level, is often reported [50]. Due to the limited number of participants showing significant coherence, no statistical tests were carried out on peak CMC strength or its corresponding frequency in the current study. The most

coherent EEG electrode sites across participants were: F3, F7, C3, FC5, FC1, and CP5. Coherence spectra yielded from the BD and DUT systems were highly concordant in terms of peak CMC strength and frequency, and width of the significant CMC. In fact, overall CMC strength was quantitatively similar between the two measurements. The significant coherence peaks occurred in the expected beta band at a mean frequency of 25.0 Hz $\pm$ 1.2 Hz for wired (BD) and 23.4 Hz $\pm$ 0.8 Hz for wireless (DUT) EEG systems across the aforementioned EEG electrodes, whereas the CMC strength was of 0.031 $\pm$ 0.019 for the BD and 0.030 $\pm$ 0.012 for the DUT, in agreement with previous studies [9], [16]. Fig. 7a shows the DUT- and BD-based CMC spectra for a single subject performing the isometric contraction. The spectra appeared very similar in terms of amplitude and spectral width. Both spectra peaked around 23 Hz, (within the beta frequency band) with comparable strengths even though the exact peak frequency differed by 2 Hz. In fact, minor inter-session variations (e.g. steadiness of the isometric contraction or alertness) within the non-simultaneous recordings may impact on the CMC spectra but appeared to fall within a normal physiological variation in the current data. Fig. 7b shows EEG scalp topographies for the CMC peaking above the primary sensorimotor cortex contralateral to the contracting hand. As expected, the CMC was focused on EEG channels over the contralateral sensorimotor cortex, peaking at C3 electrode in both EEG systems.

IV. Conclusion

The aim of this work was to design and develop a wireless Body Sensor Network allowing the synchronous acquisition of cortical (EEG) and muscular (HD-sEMG) activity for the assessment of the sensory evoked cortical responses and corticospinal coupling. The proposed system architecture is characterized by a set of Sensor Units and Synchronization Unit modules allowing to collect HD-sEMG and EEG signals in an integrated way. The developed synchronization unit allows also to integrate into the sensor network third-party devices used to provide stimuli (e.g., auditory, visual, tactile, transcranial magnetic stimulation, etc.), signals or to synchronously acquire other relevant variables (e.g., force, kinematics, etc.). The bench and experimental characterization of the system confirmed the agreement with the technical project specifications and the experimental performances observed through a wired benchmark device. Indeed, no device-specific differences were found in signal properties in terms of technical and experimental performances during conventional experimental conditions. The described experimental setups were fully wireless and did not imply any additional cabling to the subject, allowing to implement a completely wireless Body Sensor Network. Three main advantages of our system architecture with respect to the State of the Art technology for EEG and sEMG acquisition [51], [52] (MuoviPro, OT Bioelettronica, Italy) (SAGA, TMSi, The Netherlands) can be identified: (i) Modular architecture: Sensor Units do not require the use of a custom-made receiver to transfer data to the PC. Indeed, each SUs directly and independently transfer data to the receiver. Also the SyncU modules are completely independent from the receiver as they act only as a transmitter/receiver of synchronization pulses. (ii) Portability to different platforms such as PC, Smartphone, Tablet, Single Board Computers (e.g. Raspberry PI). Most of the previously cited systems transfer data exclusively to a PC through an ad-hoc receiver wired-connected to it, thus limiting the use of such devices to laboratory environments and standard protocols (e.g. walking on treadmill). On the contrary, the possibility to use a portable receiver allows the biopotential acquisition also during naturalistic tasks (e.g. free walking etc.). (iii) Synchronization: the proposed synchronization system ensures synchronization delays lower than the sampling period. Furthermore, our synchronization modules allow to synchronize the SUs with external, third-party devices (e.g. used for the study of evoked potentials) still maintaining a fully wireless system architecture. Other devices do have the possibility to interface with third party devices, but only through a cabled connection between the ad-hoc receiver and the device to be synchronized. Given the particular system architecture and the good quality of the collected signals, the proposed device represents an advancement of the State-of-the-Art technology regarding the simultaneous acquisition of EEG and HD-sEMG. Furthermore, the developed wBSN, thanks to its modularity and reduced size, represents an enabling technology to extend the investigation of the sensorimotor integration and of corticospinal coupling in addition to static conditions during more dynamic and naturalistic tasks and environments.

Acknowledgment

The authors would like to thank Phoenix PCB S.r.l. (Ivrea, Italy) for the support in PCBs production and mounting.

References

[1] E. Lattari *et al.*, "Corticomuscular coherence behavior in fine motor control of force: A critical review," *Rev. Neurol.*, vol. 51, no. 10, pp. 610–623, 2010.

[2] G. Abbruzzese and A. Berardelli, "Sensorimotor integration in movement disorders," *Movement Disorders*, vol. 18, no. 3, pp. 231–240, Mar. 2003.

[3] H. Piitulainen, S. Seipäjärvi, J. Avela, T. Parviainen, and S. Walker, "Cortical proprioceptive processing is altered by aging," *Frontiers Aging Neurosci.*, vol. 10, pp. 1–13, Jun. 2018.

[4] E. Seiss, P. Praamstra, C. Hesse, and H. Rickards, "Proprioceptive sensory function in Parkinson's disease and Huntington's disease: Evidence from proprioception-related EEG potentials," *Exp. Brain Res.*, vol. 148, no. 3, pp. 308–319, Feb. 2003.

[5] C. Pizzolato *et al.*, "Non-invasive approaches to functional recovery after spinal cord injury: Therapeutic targets and multimodal device interventions," *Exp. Neurol.*, vol. 339, May 2021, Art. no. 113612.

[6] A. Herwig, W. Prinz, and F. Waszak, "Two modes of sensorimotor integration in intention-based and stimulus-based actions," *Quart. J. Exp. Psychol.*, vol. 60, no. 11, pp. 1540–1554, Oct. 2007.

[7] M. De Tommaso, E. Vecchio, K. Ricci, A. Montemurno, D. De Venuto, and V. F. Annese, "Combined EEG/EMG evaluation during a novel dual task paradigm for gait analysis," in *Proc. 6th IEEE Int. Work. Adv. Sensors Interface (IWASI)*, Jun. 2015, pp. 181–186.

[8] R. Bortel and P. Sovka, "EEG–EMG coherence enhancement," *Signal Process.*, vol. 86, no. 7, pp. 1737–1751, 2006.

[9] H. Piitulainen, A. Botter, M. Bourguignon, V. Jousmäki, and R. Hari, "Spatial variability in cortex-muscle coherence investigated with magnetoencephalography and high-density surface electromyography," *J. Neurophysiol.*, vol. 114, no. 5, pp. 2843–2853, 2015.

[10] J. Ibáñez, A. Del Vecchio, J. C. Rothwell, S. N. Baker, and D. Farina, "Only the fastest corticospinal fibers contribute to β corticomuscular coherence," *J. Neurosci.*, vol. 41, pp. 1–42, Jun. 2021.

[11] D. Farina, A. Holobar, R. Merletti, and R. M. Enoka, "Decoding the neural drive to muscles from the surface electromyogram," *Clin. Neurophysiol.*, vol. 121, no. 10, pp. 1616–1623, Oct. 2010.

[12] R. Merletti, A. Holobar, and D. Farina, "Analysis of motor units with high-density surface electromyography," *J. Electromyogr. Kinesiol.*, vol. 18, pp. 879–890, Dec. 2008.

[13] D. F. Stegeman, B. U. Kleine, B. G. Lapatki, and J. P. Van Dijk, "High-density surface EMG: Techniques and applications at a motor unit level," *Biocybern. Biomed. Eng.*, vol. 32, no. 3, pp. 3–27, 2012.

[14] R. Merletti, M. Aventaggiato, A. Botter, A. Holobar, H. Marateb, and T. M. M. Vieira, "Advances in surface EMG: Recent progress in detection and processing techniques," *Crit. Rev. Biomed. Eng.*, vol. 38, no. 4, pp. 305–345, 2010.

[15] R. Merletti and G. L. Cerone, "Tutorial. Surface EMG detection, conditioning and pre-processing: Best practices," *J. Electromyogr. Kinesiol.*, vol. 54, Oct. 2020, Art. no. 102440.

[16] C. van de Steeg, A. Daffertshofer, D. F. Stegeman, and T. W. Boonstra, "High-density surface electromyography improves the identification of oscillatory synaptic inputs to motoneurons," *J. Appl. Physiol.*, vol. 116, no. 10, pp. 1263–1271, 2014.

[17] S. Debener, F. Minow, R. Emkes, K. Gandras, and M. De Vos, "How about taking a low-cost, small, and wireless EEG for a walk?" *Psychophysiology*, vol. 49, no. 11, pp. 1617–1621, 2012.

[18] Y. Xie *et al.*, "Novel wearable sensors for biomechanical movement monitoring based on electromagnetic sensing techniques," *IEEE Sensors J.*, vol. 20, no. 2, pp. 1019–1027, Jan. 2020.

[19] G. L. Cerone, A. Botter, and M. Gazzoni, "A modular, smart, and wearable system for high density sEMG detection," *IEEE Trans. Biomed. Eng.*, vol. 66, no. 12, pp. 3371–3380, Dec. 2019.

[20] A. Delorme *et al.*, "EEGLAB, SIFT, NFT, BCILAB, and ERICA: New tools for advanced EEG processing," *Comput. Intell. Neurosci.*, vol. 2011, pp. 1–12, Oct. 2011.

[21] A. Ojeda, N. Bigdely-Shamlo, and S. Makeig, "MoBILAB: An open source toolbox for analysis and visualization of mobile brain/body imaging data," *Frontiers Hum. Neurosci.*, vol. 8, p. 121, Mar. 2014.

[22] R. R. Harrison and C. Charles, "A low-power low-noise CMOS amplifier for neural recording applications," *IEEE J. Solid-State Circuits*, vol. 38, no. 6, pp. 958–965, Jun. 2003.

[23] *CC1310 SimpleLink TM Ultra-Low-Power Sub-1 GHz Wireless MCU*, Texas Instrum., Dallas, TX, USA, 2018, vol. 68.

[24] *RHD2000 Series Digital Electrophysiology Interface Chips-Datasheet*, Intan Technol. LLC, Los Angeles, CA, USA, 2013, pp. 1–38.

[25] A. C. Metting van Rijn, A. Peper, and C. A. Grimbergen, "High-quality recording of bioelectric events—Part 1 interference reduction, theory and practice," *Med. Biol. Eng. Comput.*, vol. 28, no. 5, pp. 389–397, Sep. 1990.

[26] E. M. Spinelli, M. A. Mayosky, and R. Pallas-Areny, "A practical approach to electrode-skin impedance unbalance measurement," *IEEE Trans. Biomed. Eng.*, vol. 53, no. 7, pp. 1451–1453, Jul. 2006.

[27] M. Haberman, A. Cassino, and E. Spinelli, "Estimation of stray coupling capacitances in biopotential measurements," *Med. Biol. Eng. Comput.*, vol. 49, no. 9, pp. 1067–1071, Sep. 2011.

[28] G. Piervirgili, F. Petracca, and R. Merletti, "A new method to assess skin treatments for lowering the impedance and noise of individual gelled Ag–AgCl electrodes," *Physiol. Meas.*, vol. 35, no. 10, pp. 2101–2118, Oct. 2014.

[29] R. C. Oldfield, "The assessment and analysis of handedness: The Edinburgh inventory," *Neuropsychologia*, vol. 9, no. 1, pp. 97–113, Mar. 1971.

[30] R. Hari and A. Puce, *MEG-EEG Primer*. Oxford, U.K.: Oxford Univ. Press, 2017.

[31] R. Oostenveld, P. Fries, E. Maris, and J.-M. Schoffelen, "FieldTrip: Open source software for advanced analysis of MEG, EEG, and invasive electrophysiological data," *Comput. Intell. Neurosci.*, vol. 2011, pp. 1–9, Oct. 2011.

[32] A. Gramfort, "MEG and EEG data analysis with MNE-Python," *Frontiers Neurosci.*, vol. 7, pp. 1–13, Dec. 2013.

[33] T. Allison, G. McCarthy, C. C. Wood, P. D. Williamson, and D. D. Spencer, "Human cortical potentials evoked by stimulation of the median nerve. II. Cytoarchitectonic areas generating long-latency activity," *J. Neurophysiol.*, vol. 62, no. 3, pp. 711–722, Sep. 1989.

[34] B. A. Brett-Green, L. J. Miller, W. J. Gavin, and P. L. Davies, "Multisensory integration in children: A preliminary ERP study," *Brain Res.*, vol. 1242, pp. 283–290, Nov. 2008.

[35] T. M. Vieira, R. Merletti, and L. Mesin, "Automatic segmentation of surface EMG images: Improving the estimation of neuromuscular activity," *J. Biomech.*, vol. 43, no. 11, pp. 2149–2158, Aug. 2010.

[36] H. Piitulainen, T. Rantalainen, V. Linnamo, P. Komi, and J. Avela, "Innervation zone shift at different levels of isometric contraction in the biceps brachii muscle," *J. Electromyogr. Kinesiol.*, vol. 19, no. 4, pp. 667–675, 2009.

[37] J. T. Gwin and D. P. Ferris, "Beta- and gamma-range human lower limb corticomuscular coherence," *Frontiers Hum. Neurosci.*, vol. 6, p. 258, Sep. 2012.

[38] V. M. McClelland, Z. Cvetkovic, and K. R. Mills, "Modulation of corticomuscular coherence by peripheral stimuli," *Exp. Brain Res.*, vol. 219, no. 2, pp. 275–292, Jun. 2012.

[39] F. Negro, K. Keenan, and D. Farina, "Power spectrum of the rectified EMG: When and why is rectification beneficial for identifying neural connectivity?" *J. Neural Eng.*, vol. 12, no. 3, Jun. 2015, Art. no. 036008.

[40] D. M. Halliday, J. R. Rosenberg, A. M. Amjad, P. Breeze, B. A. Conways, and S. F. Farmer, "A framework for the analysis of mixed time series/point process data—Theory ad application to the study of physiological tremor, single motor unit discharges and electromyograms," *Prog. Biophys. Mol. Biology.* vol. 64, pp. 237–278, Oct. 1995.

[41] M. Illman, K. Laaksonen, M. Liljeström, V. Jousmäki, H. Piitulainen, and N. Forss, "Comparing MEG and EEG in detecting the ~20-Hz rhythm modulation to tactile and proprioceptive stimulation," *NeuroImage*, vol. 215, Jul. 2020, Art. no. 116804.

[42] H. Piitulainen, M. Bourguignon, X. De Tiège, R. Hari, and V. Jousmäki, "Coherence between magnetoencephalography and hand-action-related acceleration, force, pressure, and electromyogram," *NeuroImage*, vol. 72, pp. 83–90, May 2013.

[43] M. Bourguignon *et al.*, "Functional motor-cortex mapping using corticokinematic coherence," *NeuroImage*, vol. 55, no. 4, pp. 1475–1479, Apr. 2011.

[44] R. Merletti, M. Aventaggiato, A. Botter, A. Holobar, H. Marateb, and T. M. M. Vieira, "Advances in surface EMG: Recent progress in detection and processing techniques," *Crit. Rev. Biomed. Eng.*, vol. 38, no. 4, pp. 45–305, 2010.

[45] B. B. Winter and J. G. Webster, "Driven-right-leg circuit design," *IEEE Trans. Biomed. Eng.*, vol. BME-30, no. 1, pp. 62–66, Jan. 1983.

[46] M. R. Keshtkaran and Z. Yang, "A fast, robust algorithm for power line interference cancellation in neural recording," *J. Neural Eng.*, vol. 11, no. 2, pp. 1–14, 2014.

[47] D. T. Mewett, K. J. Reynolds, and H. Nazeran, "Reducing power line interference in digitised electromyogram recordings by spectrum interpolation," *Med. Biol. Eng. Comput.*, vol. 42, no. 4, pp. 524–531, Jul. 2004.

[48] A. Botter and T. M. Vieira, "Filtered virtual reference: A new method for the reduction of power line interference with minimal distortion of monopolar surface EMG," *IEEE Trans. Biomed. Eng.*, vol. 62, no. 11, pp. 2638–2647, Nov. 2015.

[49] J. G. Webster, *Medical Instrumentation: Application and Design*. Hoboken, NJ, USA: Wiley, 2013.

[50] M. Pohja, S. Salenius, and R. Hari, "Reproducibility of cortex–muscle coherence," *NeuroImage*, vol. 26, no. 3, pp. 764–770, Jul. 2005.

[51] K. Petkos *et al.*, "A high-performance 8 nV/$\sqrt{}$Hz 8-channel wearable and wireless system for real-time monitoring of bioelectrical signals," *J. NeuroEng. Rehabil.*, vol. 16, no. 1, pp. 1–24, Dec. 2019.

[52] W. Song *et al.*, "Design of a flexible wearable smart sEMG recorder integrated gradient boosting decision tree based hand gesture recognition," *IEEE Trans. Biomed. Circuits Syst.*, vol. 13, no. 6, pp. 1563–1574, Dec. 2019.